Theoretical Investigation of the Surface Reaction $N_{(ads)} + H_{(ads)} \rightarrow NH_{(ads)}$ on Ru(0001) Using Density Functional Calculations, Variational Transition-State Theory, and Semiclassical Tunneling Method

Alessandro Volpi and David C. Clary*

Physical and Theoretical Chemistry Laboratory, University of Oxford, South Parks Road, Oxford OX1 3QH, United Kingdom

Received: July 23, 2003; In Final Form: October 12, 2003

The title reaction is an important step in the synthesis of ammonia over ruthenium-based catalysts, which have recently received increasing attention. The study presented here is fully theoretical and uses a reduced dimensionality approach to the surface reaction. A potential energy surface is first obtained by density functional calculations using a supercell approach. We have then calculated rate constants in the range of temperature 200−1000 K, which includes the temperature at which the ammonia production is usually performed. This has been done within the framework of variational transition-state theory in a reaction-path formulation, comparing different levels of theory and including quantum transmission and reflection effects by semiclassical methods. Calculated rates are fitted by the Arrhenius law. Finally, we have carried out an accurate investigation of the isotopic effect by replacing hydrogen with deuterium.

1. Introduction

Chemical reactions occurring at surfaces are extremely common, both for industrial synthesis (heterogeneous catalysis employing surfaces is used in 90% of the manufacturing processes[1]) and in nature, for instance, in the case of important atmospheric reactions. Even in astrochemistry, the most abundant interstellar molecule, H_2, can be formed at the surface of grains.[2]

Surface reactions are often multistep processes. Therefore, the general strategy to understand the mechanism is to investigate first single steps and then use them in building up realistic kinetics models of the overall processes. In this paper, we are concerned with one of the steps taking place in the industrial production of ammonia, which has a crucial importance in itself, as well as a basis for the production of other chemicals. Traditionally, the synthesis of ammonia was performed using iron-based catalysts,[3] but then attention was also turned to ruthenium which, being less inhibited by ammonia, shows a larger activity than iron and allows operation at greater pressures.[4,5] Our study will deal with a ruthenium-based catalyst.

Ammonia industrial synthesis requires very severe conditions of temperature (more than 400 °C) and pressure (more than 100 bar). A substantial amount of work has been done both theoretically and experimentally to achieve a better comprehension of the steps through which ammonia production proceeds. It is understood that the strong N−N bond of the nitrogen molecule is broken in the first place in a dissociative adsorption step.[6−11] There follow three subsequent hydrogenation steps, which finally lead to the formation of the NH_3 molecule. The dissociative adsorption has been investigated more deeply than the stepwise addition reactions, for which a full and exhaustive description is still needed. Microkinetic analysis of the overall synthetic process has also been performed.[12,13]

On the experimental side, the close-packed Ru(0001) surface has been investigated in many different contexts. Besides the mentioned bond breaking of the nitrogen molecule.[7,14−16] these studies included spectroscopical probe of the interaction properties between adsorbates[17] and the ammonia synthesis itself.[18] The study of both geometric and energetic adsorption features of atomic and molecular species on the Ru(0001) surface has also received considerable attention and will be discussed later because it is relevant to the approach we will present here.

On the theoretical side, most of the efforts have been devoted to electronic structure aspects. Considerable attention has been dedicated to what is considered as the rate-determining step of the reaction, that is, the dissociation of the N_2 molecule with adsorption of the two atoms on the metal surface.[19,20] It has been proved that a stepped surface provides a much more convenient reaction path with respect to terraces with a huge difference in the activation energy,[21] which leads to a difference of 9 orders of magnitudes for the adsorption rate. This is the result of a combination of electronic and geometrical effects. Few works have dealt with the entire synthetic process, calculating intermediates, transition states, and activation energies for each step,[22−24] but without addressing the issue of the calculation of reaction rates. The possibility of a metal surface catalyzed process running under softer conditions of temperature and pressure, like the synthesis performed in nature by the enzyme nitrogenase, was also addressed.[16] Despite this amount of work about electronic structure and reaction paths, surprisingly not much has been done as far as the determination of rate constants for single steps is concerned: only few estimates are available, and sometimes different investigators disagree even on which one is the rate-limiting step of the global synthesis.

* To whom correspondence should be addressed. E-mail: david.clary@chem.ox.ac.uk.

10.1021/jp0361475 CCC: $27.50
Published on Web 12/10/2003

In this context, it is evident that a computational study of the reaction rates for the various steps would be greatly desirable. As a first contribution in this sense, we investigate one of the hydrogenation steps of the ammonia synthesis, namely,

$$N_{(ads)} + H_{(ads)} \rightarrow NH_{(ads)} \quad (1)$$

In the reaction above, two adsorbed atoms can migrate and react to give an NH molecule that is still adsorbed on the surface. This is the first bond-formation process in the ammonia synthesis.

To achieve our goal, we need, first of all, a realistic description of the interaction potential of the adsorbates with each other and with the metal surface. A potential energy surface (PES) has been determined by density functional theory (DFT) calculations. We have followed a reduced dimensionality approach, which allows us to partially eliminate the complexity of the problem by freezing some of the degrees of freedom. Of course, this choice must be made carefully to not lose the main features of the physics of the system and to provide a realistic description of the reaction. The choice of the coordinates to be employed in the description of the system and the details regarding our DFT calculations are discussed in section II.

Once a PES is obtained, this reaction can be treated without the complications arising from the inherent heterogeneous phase features of the investigated system. For the dynamics study, we have adopted variational transition-state theory (TST). Variational TST has been tested in a number of different problems, which gives confidence in its reliability for the application to the present system (for an exhaustive review, see ref 25). This picture combines the advantages of being relatively simple and allowing for the inclusion of quantal effects, which are expected to be important because we are concerned with the diffusion of atomic hydrogen on a metal surface. The theory and the specifications of the particular TST version that we use in this paper are given in section III.

Our rate constants results are presented and discussed in section IV, together with a study of the isotopic effect when hydrogen is replaced by deuterium. Conclusions, perspectives, and possible refinements of the work presented here follow in the final section V.

2. The Interaction Potential

2.1. Choice of the Coordinates. Our aim is to describe a chemical reaction occurring between adsorbates on a surface. Throughout this paper, we will consider a close-packed hexagonal Ru(0001) surface, and we will be concerned with a flat surface, that is, the reaction will take place on a terrace. This choice is supported by findings in refs 23 and 24. In those works, reactions on flat and stepped surfaces are analyzed and compared, the outcome being that stepwise hydrogenation reactions (and particularly the one that we are interested in) are not strongly affected by the presence of steps,which do not cause a dramatic change in the reaction barrier height. Bearing in mind the N_2 dissociative adsorption reaction, this may look somewhat unexpected: in that case, the reaction mechanism is dominated by steps, which exhibit a much smaller activation energy and basically provide the only viable way for the reaction to occur. The reason for that is the bonding competition for the same Ru atom that the two N atoms in N_2 undergo in the transition state (TS) of the flat surface reaction. This does not occur in the presence of a step, which, providing another metal atom, makes the sharing unnecessary. The same idea applies in principle to the hydrogen addition reactions, but in fact, the the H−Ru bond is much weaker than N−Ru, resulting in a smaller overall effect. The energetics of the reaction is not dramatically affected by steps, and a flat surface is definitely a reliable model to represent the process.

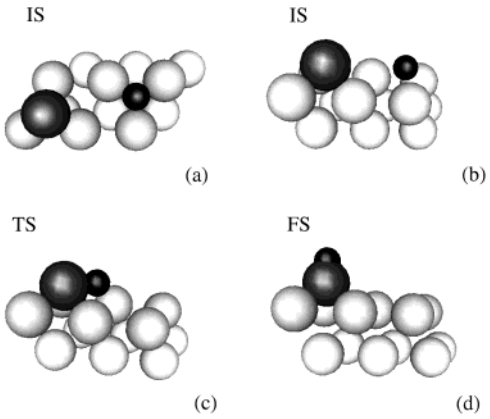

Figure 1. (a) Top view of the unit cell used for the DFT calculations. The initial state is shown with the N atom adsorbed on a hcp site and the H atom coadsorbed in an adjacent fcc site. Panels b, c, and d show a side view of the cell for the initial, transition, and final states, respectively. In all panels, white and light gray atoms are Ru atoms of the lower and upper layer of the unit cell, while dark gray and black are used for N and H, respectively.

To obtain a tractable model, the first assumption to make is considering a rigid substrate. This approximation is almost unavoidable given the increase of computer time needed for allowing surface-atom relaxation. However, in principle, we still have to deal with six degrees of freedom to provide a full description of the motion of the N and H atoms on the metal surface. A six-dimensional PES would require an unsustainable computational cost for the calculation of the ab initio points and for the subsequent fit procedure, raising then the problem of how to simplify the approach to the problem. This goal can be achieved by combining a reduced dimensionality and all available information on the reaction path. It is convenient to focus first on the initial and final states of the surface reaction, exploiting a series of existing results to characterize optimized structures and geometries for pure adsorption systems, that is, N/Ru, H/Ru, and NH/Ru. It has been proved both theoretically[26] and experimentally[27] that atomic nitrogen occupies preferentially hcp hollow sites and forms a strong bond with the Ru surface. Hydrogen atoms prefer as well 3-fold hollow sites.[28,29] In choosing the initial state, we have to place both atoms in the reference unit cell that we will employ in our DFT calculations, which we anticipate to be a (2×3) surface unit cell. Zhang and co-workers[23] have determined that the most stable initial state is the one with N chemisorbed in a hcp site and H coadsorbed in an adjacent fcc site [see Figure 1, panels a and b]. This choice provides the maximum separation and the minimum bonding competition between the coadsorbates.

Also for the location of the final state, we can take advantage of existing studies. The NH adsorption site has been investigated by infrared spectroscopy and DFT calculations.[30] The finding of that work was that the energetically favorable adsorption geometry for NH is at the hcp 3-fold hollow site with the N−H axis perpendicular to the surface. This preference was confirmed by a vibrational analysis of the NH + H coadsorbed system.[31]

The initial and final states of the hydrogenation are then well understood. In addition, ref 23 provides a study of structure and geometry of the reaction transition state. In particular, the authors were able to single out three possible TSs, the most

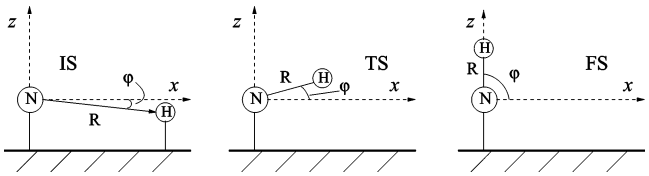

Figure 2. Structure and geometry of initial (IS), transition (TS), and final (FS) states for the reaction $N_{(ads)} + H_{(ads)} \rightarrow NH_{(ads)}$ in the adopted two-dimensional space representation. Values of distances and angles are highlighted for each configuration, together with our choice for the orientation of the (x, z) reference frame.

stable of which is the so-called hcp-based, where N occupies a position very close to the original hcp site and H is getting closer along the direction of the initial interatomic distance. This gives reasons for reducing the number of degrees of freedom maintaining at the same time a realistic description of the process. It is reasonable to assume that the nitrogen atom stays fixed during the reaction, while the mobile hydrogen atom is migrating over the surface.

This approach eliminates all of the nitrogen degrees of freedom. However, a further simplification of the problem is possible by adopting polar coordinates centered on N and observing that only the interatomic distance R between N and H and the azimuthal angle ϕ are really needed for a description of the reactive event (see Figures 1 and 2). The other angular degree of freedom (i.e., the rotational motion of H parallel to the metal surface) would refine the description of the reaction, possibly opening alternative reaction paths. However, it can be neglected at this stage and eventually included in future refinements of the work presented here. In force of this argument, our strategy will be to calculate a PES as a function of the two coordinates R and ϕ and to perform a search of the reaction minimum energy path (MEP) in this reduced two-dimensional space. This is needed, as will be discussed later in greater detail, for the application of the TST.

It is worthwhile to point out two aspects at this stage: First, our approach is rigorous for the reactants because it is based on the configuration of the initial state, whereas it is less accurate for the final state, where NH adsorption height would vary (as will be discussed) with respect to the one of the isolated N atoms. However, in the TST description of the reactive event, it is crucial to have an accurate representation of reactants and transition state, so this difference of accuracy will not be a main drawback. Second, the quality of our approximation can be tested to some extent by comparing the energetics of the reaction obtained with our approach with the one calculated by Zhang et al.[23] or by Logadottir and Nørskov,[24] who treated all the degrees of freedom and presumably found a very good estimate, within the DFT limits, of exothermicity and barrier height.

2.2. DFT Calculation of the Potential Energy Surface. The ab initio points of the PES have been obtained by a DFT calculation. We have used the open-source software named DACAPO developed at the Center for Atomic and Molecular Physics, Copenhagen, Denmark.[32]

Wave functions were expanded on a plane wave basis set with energy up to 340 eV. A RPBE description of exchange and correlation effects[33] and ultrasoft pseudopotentials[34] were adopted. Self-consistent electron density was obtained by iterative diagonalization of the Kohn−Sham Hamiltonian. Fermi broadening of the occupation numbers was done with a width of 0.2 eV. The resulting density was mixed using a Pulay charge-mixing method.[35]

The supercell approach was employed to model the periodic geometry of the Ru(0001) surface. In particular, we chose a periodic array of two layer slabs and a (2×3) unit cell. The atoms of the metal substrate were kept fixed at bulk positions (these approximations were successfully tested in previous papers[23,24]).

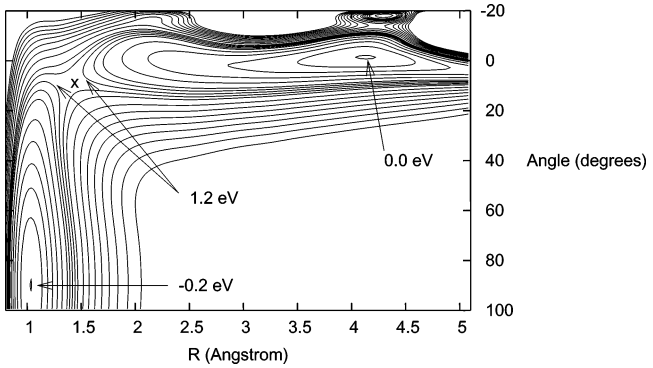

Figure 3. Contour plot representation of the calculated PES for the title reaction as a function of the interatomic distance R and of the ϕ angle. The overall zero of the surface is indicated and corresponds to the reactants configuration. Contour lines are placed from −0.2 to 1.0 eV every 0.2 eV, then every 0.1 till 1.4 eV, and then again every 0.2 till 3.0 eV. The "x" is the location of the saddle point.

The lattice constant was set to 2.7 Å and the distance between slabs to ∼11 Å. An 18 K-points 1×1 Chadi−Cohen set[36] was used to sample the hexagonal Ru surface Brillouin zones.

With these settings, we have calculated the potential on a fine rectangular grid of R and ϕ points. We have selected 20 R values ranging from 0.8 to 5.1 Å, and 16 ϕ points from −20 ° to 100 ° (for the definition of our set of coordinates, see Figure 2). That the coordinate ranges spanned by our calculations are large enough to describe the all reactive process becomes evident if the geometry of initial, final, and transition states are considered. The initial state was found by letting the two coadsorbed atoms relax. To this purpose, we used a Polak−Ribiere conjugate gradient algorithm for ionic minimization. The resulting adsorption heights were 1.24 and 1.11 Å for N and H in the hcp and fcc adjacent sites, respectively, in reasonable agreement both with ref 24 (1.19 and 1.08 Å), in which the same numerical code but slightly different settings were used, and with ref 23 (1.09 and 1.05 Å), in which a different numerical code was employed.

A PES has then been generated by fitting the ab initio points with bicubic splines. This choice gives us the double advantage of allowing the use of standard numerical libraries and ensuring the existence of continuous second derivatives of the analytical fitting function, the latter being a necessary ingredient for the dynamical method that we will use in this work.

In Figure 3, we show a contour plot of the potential surface that we have calculated. Reactants and products valleys are well distinguishable, as well as the saddle point region. The initial state, with N being in the hcp site and H in an adjacent fcc site, corresponds to $R = 4.13$ Å and $\phi = -1.80°$. The final state is not allowed to relax in our model because N is kept fixed. As a consequence, its energy and geometry are not optimized. However, ϕ equals 90° in the final state, proving that the most stable configuration is the one with the N−H bond axis perpendicular to the metal surface. According to Zhang and co-workers,[23] at the transition state the N−H distance has reduced to 1.40 Å.

3. Theory

3.1. TST Expression of the Rate Constants. We apply variational transition-state theory in a reaction-path formulation

for the calculation of thermal rate constants for the process 1. This will be combined with a semiclassical calculation of multidimensional tunneling probabilities. We follow the procedure described by Truhlar and co-workers.[37−41] In particular, given the similarity with the problem treated here, our work will be based on ref 42, which explicitly dealt with diffusion of H and isotopic variants on a Cu surface. This formalism has been applied as well to an atomic diffusion problem on Ru(0001).[43]

In the present method, the motion of the adsorbed H atom is conveniently described in Cartesian coordinates relative to the N atom. Given the particular restrictions of our approach, we choose a reference frame with the x axis oriented like the projection on the surface of R in the initial state (reactants). The z axis is perpendicular to the surface (see Figure 2). The following relations hold:

$$R^2 = x^2 + z^2$$
$$\tan\phi = z/x \qquad (2)$$

The advantage of this choice is that the motion in the (R, ϕ) space can be rigorously replaced by the motion in (x, z) space, the y coordinate being always equal to 0. This will simplify equations and computational procedure.

First of all, the saddle point of the reaction needs to be located. In general, this might be an hard task to perform, but it is straightforward in our two-dimensional case. The saddle point is found via the solution of $\nabla V = 0$, where V is our PES, and turns out to be located at $R = 1.39$ Å and $\phi = 8.60°$ and to lie 1.26 eV above the reactants potential energy. We notice here that this finding is in good agreement with refs 23 and 24, which predicted a barrier height of 1.13 and 1.2 eV, respectively, but relaxing all N and H degrees of freedom. This is an indication of the suitability of our reduced set of coordinates to describe the essential features of the process.

In the procedure adopted here, first the MEP of the reaction is found as the path of steepest descents of the Born−Oppenheimer PES from the saddle point to reactants and products. Then we consider generalized transition states as coordinate space dividing surfaces, which are planes in the two-dimensional coordinate system of H and are perpendicular to the MEP at each intersection. The existence of such a surface (or its generalization to the phase space) is one of the fundamental assumptions of TST, together with the so-called no-recrossing hypothesis, according to which trajectories originated at the reactants and passing through this dividing surface in the products direction will not recross the surface. To some extent, we will consider a correction to this assumption in the calculation of the transmission coefficient.

The reaction coordinate s is defined as the arc length along the MEP in (x, z) space, so that its value equals 0 at the saddle point. The value of s parametrizes generalized TST dividing surfaces along the MEP. For each of these surfaces, the classical mechanical rate constant is the equilibrium one-way coefficient of trajectories passing through the surface in the products direction or, in other words, the number of crossing states coming from the reactants site per unit time divided by the number of occupied reactant states. The explicit expression for the generalized TST classical rates, at given temperature T and reaction coordinate s, reads[44]

$$k^{GT}(T,s) = \frac{\sigma}{\beta h}\frac{Q^{GT}(T,s)}{Q^{R}(T)}\exp[-\beta V_{MEP}(s)] \qquad (3)$$

where $\beta = (k_B T)^{-1}$, k_B being the Boltzmann's constant, h the Planck's constant, V_{MEP} the potential energy on the MEP at s, and σ the symmetry factor,[45] which in the present case must be interpreted as the number of paths from equivalent reactants sites to adjacent products sites and equals 3 given the hexagonal structure of the Ru(0001) surface (this becomes evident by repeating in (x, y) space the unit cell of Figure 1). A special discussion must be devoted to the partition function for the dividing surface at s, Q^{GT}, and for the reactants, Q^{R}, because they can be calculated in alternative ways giving different levels of description of the vibrational degrees of freedom orthogonal to the MEP and of the reactants. Before discussing this, it is important to point out the peculiarity of variational TST. The rate constant is obtained by a minimization process by varying the position of the dividing surface along the MEP:

$$k^{CVT}(T) = \min_s k^{GT}(T, s) \qquad (4)$$

In the present scheme, we distinguish between quantal effects along the reaction coordinate and quantal effects orthogonal to the reaction coordinate. The former are included by multiplying k^{CVT} by a ground-state transmission coefficient and will be discussed below. The latter are related to the expression that we choose for the partition functions in eq 3. Partition functions can be expressed as the products of an electronic term times a vibrational one (neither electronic excited states nor the metallic features of the surface substrate will be considered here). We consider the ratio $Q_{el}^{GT}(T, s)/Q_{el}^{R}(T)$ to be equal to 1. As for the vibrational part, a normal-mode analysis needs to be performed, leading to the calculation of the harmonic force constants. The partition functions can be calculated either classically (classical harmonic oscillator, CHO) or quantally. In the second case, a quantum harmonic oscillator (QHO) approximation or a full quantum treatment including anharmonicity to calculate the energy levels of the normal modes can be adopted. We solve the quantum eigenvalue problem using a discrete variable representation approach, namely, the Fourier grid (FG) method (see refs 46 and 47 for an exhaustive description of the method). Although grid points can in principle be adapted to any shape of the potential, in this case, a simple linear grid is found to be numerically efficient.

For the reactants, we treat the two normal modes in the context of the independent normal-mode approximation and then simply express the total partition function as a product of the two resulting terms.

The matter is slightly more complicated for the generalized transition state, and it is related to the method followed for the identification of the MEP (again, only the general ideas are given here, and we refer to ref 42 for a more exhaustive discussion). We start at the saddle point calculating the force constant matrix $\mathbf{F}$ with respect to the Cartesian coordinates (x, z), the diagonalization of which gives one positive and one negative eigenvalue. The eigenvector corresponding to the negative eigenvalue (i.e., to the imaginary frequency) is used to compute the first pair of points along the MEP, one in the direction of the reactants and one in the direction of the products. This is achieved taking steps of $\pm\Delta s$ in the direction of the mentioned eigenvector. Subsequent steps are then taken in the direction of the negative gradient for both sides of the MEP. At each step, the normal mode (in our two-dimensional case, only one degree of freedom is left after separating the reaction coordinate) orthogonal to the MEP is extracted by the projection method developed by Miller et al. for gas-phase reactions.[48] Once the normal mode is extracted, generalized transition-state partition

functions can be calculated as a function of s (and T, of course) using the mentioned three possible approaches (CHO, QHO, FG).

It is worthwhile to notice that the present method could be very readily generalized to a higher number of coordinates, the formalism remaining exactly the same as in the present two-dimensional study. In the case of the reactants, we will have always to deal with one more degree of freedom than for the generalized TS, for which one degree of freedom (namely. the reaction coordinate) is separated out.

3.2. Quantal Effects along the Reaction Coordinate. As pointed out above, one of the basic assumptions of TST is that the reaction coordinate can be separated from the other degrees of freedom of the system. Of course, this applies as well to quantal effects, and we distinguish between quantal effects orthogonal to the MEP, which are taken into account choosing a quantum representation of the partition functions for reactants and generalized transition state, and quantal effects on the motion along the reaction coordinate. The latter have to account for nonclassical reflection at energies above the barrier height, as well as for nonclassical transmission through the potential barrier. This is accomplished by multiplying the rate constants $k^{\mathrm{CVT}}(T)$ by a ground-state transmission coefficient of the form[37,42,44,49,50]

$$c^{\mathrm{CVT/G}} = \int_{\epsilon_{\mathrm{int}}^{\mathrm{RG}}}^{\infty} P^{\mathrm{G}}(E)\exp(-\beta E)\,\mathrm{d}E \Big/ \int_{V_{\mathrm{a}}^{\mathrm{G}}[s_*^{\mathrm{CVT}}(T)]}^{\infty} \exp(-\beta E)\,\mathrm{d}E \tag{5}$$

where $V_{\mathrm{a}}^{\mathrm{G}}(s)$ is the adiabatic energy curve defined by

$$V_{\mathrm{a}}^{\mathrm{G}}(s) = V_{\mathrm{MEP}}(s) + \epsilon_{\mathrm{int}}^{\mathrm{G}}(s) \tag{6}$$

and $\epsilon_{\mathrm{int}}^{\mathrm{G}}(s)$ is the zero-point energy in the generalized TS at s. In eq 5, $s*^{\mathrm{CVT}}(T)$ is the value of the reaction coordinate for which $k^{\mathrm{GT}}(T,s)$ is minimum, E is the total energy, $\epsilon_{\mathrm{int}}^{\mathrm{RG}}$ is the zero-point energy for the reactants, and $P^{\mathrm{G}}(E)$ is the ground-state transmission probability as a function of the energy. Rate constants can then be expressed as

$$k^{\mathrm{CVT/G}} = k^{\mathrm{CVT}} c^{\mathrm{CVT/G}} \tag{7}$$

The crucial point is now the approximation to implement for the calculation of the ground-state transmission coefficient, $P^{\mathrm{G}}(E)$. Following previous works,[42,50,51] we find it convenient to use semiclassical methods, which are known to yield results within 10% of the accurate quantum value.[50,51] This is definitely enough for our purposes if one considers the level of approximation in the description of the reaction that we are providing here, due first to the inherent approximate nature of DFT calculations and second to the reduced dimensionality approach. The $P^{\mathrm{G}}(E)$ coefficient is then estimated applying a one-dimensional semiclassical approximation to the transmission probability through the vibrationally adiabatic ground-state potential, $V_{\mathrm{a}}^{\mathrm{G}}(s)$. The explicit recipe is[52]

$$P^{\mathrm{G}}(E) = \begin{cases} 0, & E < E_0, \\ \{1+\exp[2\vartheta(E)]\}^{-1}, & E_0 \le E \le V_{\mathrm{a}}^{\mathrm{AG}}, \\ 1 - P^{\mathrm{G}}(2V^{\mathrm{AG}} - E), & V_{\mathrm{a}}^{\mathrm{AG}} < E \le 2V_{\mathrm{a}}^{\mathrm{AG}} - E_0, \\ 1, & 2V_{\mathrm{a}}^{\mathrm{AG}} - E_0 < E \end{cases} \tag{8}$$

where E_0 is the quantal threshold energy, that is, $V_{\mathrm{a}}^{\mathrm{G}}$ in the reactants site (taken as the sum of the normal-mode zero-point energies) and $V_{\mathrm{a}}^{\mathrm{AG}}$ is the energy required for the vibrationally adiabatic reaction and is equal to the maximum of $V_{\mathrm{a}}^{\mathrm{G}}(s)$; finally, the imaginary-action integral is defined by

$$\vartheta(E) = \hbar^{-1}\int_{s_<}^{s_>} (2\mu_{\mathrm{eff}}(s)[V_{\mathrm{a}}^{\mathrm{G}}(s) - E])^{1/2}\,\mathrm{d}s \tag{9}$$

where $s_<$ and $s_>$ are the classical turning points, $V_{\mathrm{a}}^{\mathrm{G}}(s_<) = V_{\mathrm{a}}^{\mathrm{G}}(s_>) = E$. The mass in eq 9 deserves a closer scrutiny. If μ_{eff} is set equal to the mass of the H atom, this is equivalent to assuming no curvature of the reaction path. The corresponding coefficient corresponds to semiclassical adiabatic ground-state tunneling along the MEP and, following ref 42, will be indicated with the acronym SAG. Alternatively, one can include the path curvature, resulting in a more accurate description of the quantal effects on the reaction coordinate motion. In this work, we will consider the small curvature approach (SCSAG),[37] which is implemented by using an effective reduced mass depending on s, which is generally smaller than the mass of the moving atom. In this way, all of the effects of the reaction path curvature on the tunneling probabilities are condensed in μ_{eff}. Explicit formulas for the calculation of the effective reduced mass along the MEP are given in the literature,[37,42] and we refer to those papers for details and references.

There is a final issue that can affect the results and needs to be addressed here. The initial states of the reaction 1 correspond to a series of bound states, that is, discretized eigenvalues. The expression 5 given for the ground-state transmission coefficient is perfectly suitable for an initial state being in the continuum but should be modified to deal with the actual eigenvalues between E_0 and $V_{\mathrm{a}}^{\mathrm{AG}}$. This leads to the formula[42]

$$c^{\mathrm{CVT/QG}}(T) = \frac{\displaystyle\sum_n \frac{\mathrm{d}E_n}{\mathrm{d}n} P^{\mathrm{G}}(E_n)\exp(-\beta E_n) + \int_{V_{\mathrm{a}}^{\mathrm{AG}}}^{\infty} P^{\mathrm{G}}(E)\exp(-\beta E)\,\mathrm{d}E}{\displaystyle\int_{V_{\mathrm{a}}^{\mathrm{G}}[s_*^{\mathrm{CVT}}(T)]}^{\infty} \exp(-\beta E)\,\mathrm{d}E} \tag{10}$$

where Q stands for quantized (reactants) energy levels.

Numerical values of the rate constants yielded by all of the TST and tunneling alternative formulations presented here are discussed and compared in the next section.

4. Results

The search of the MEP starts from the saddle point ($s = 0$) and goes toward both reactants and products. We have taken an overconvergent number of points along the path (namely, 4000), which ensures rate constants convergent to the fourth digital figure in the investigated range of temperature (200−1000 K). Integrals in eqs 5, 9, and 10 were calculated using simple standard routines based on the extended trapezoidal rule.

For the calculation of the bound states of the normal modes orthogonal to the MEP (as well as for the reactants), we fixed the extremes of the potential curves in the (x, z) space according to the range spanned by our ab initio points in the (R, ϕ) space, that is, $0.8 < R < 5.1$ Å, and $-20° < \phi < 100°$. We have found that a linear grid of 500 points is enough to yield eigenvalues converged to better than 0.01%.

We remind the reader that the reaction coordinate is defined as the arc length in the (x, z) plane where the motion takes place. It starts from the saddle point ($s = 0$) and ranges from $s = -2.77$ Å (reactants side) to $s = 1.66$ Å (products side). In Figure 4, we show the trajectory of the MEP both in the (R, ϕ) and in

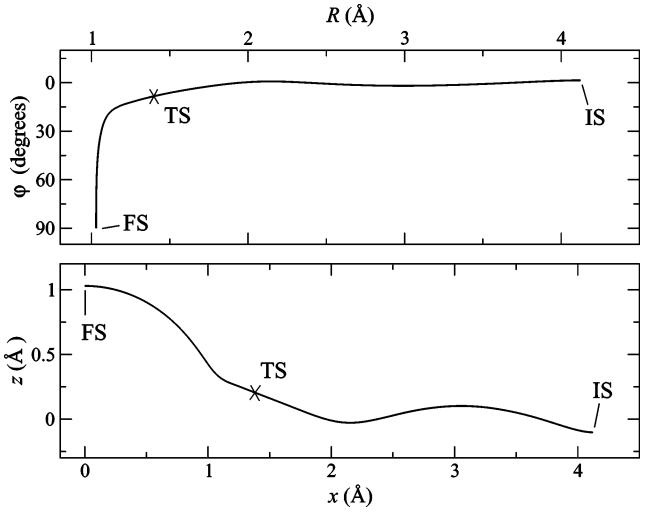

Figure 4. MEP trajectory in the (R, ϕ) space (a) and in the (x, z) space (b). Locations of initial, transition, and final states are indicated.

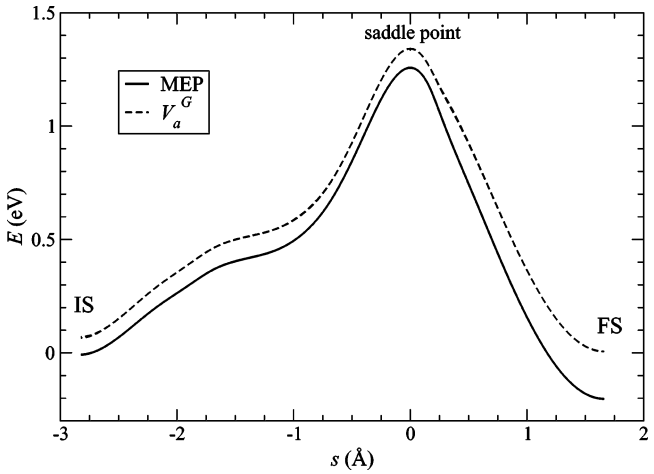

Figure 5. Minimum energy path for the title reaction as a function of the reaction coordinate s. The vibrationally adiabatic ground-state potential, $V_a^G(s)$ is also shown, both for the full quantum treatment and for the harmonic oscillator approximation. The zero-point energies obtained with the two methods are very close and cannot be distinguished on this scale.

the (x, z) space. Large R and a small negative ϕ correspond to the reactants state. Then R decreases approaching the equilibrium distance for the adsorbed NH molecule, while ϕ is flipping to 90°, the most stable configuration for NH, with the interatomic axis orthogonal to the surface. It is clear that the interatomic distance R is close to the reaction coordinate in the reactants side, where ϕ only undergoes small variations. After the TS, the weight of the variable ϕ on the reaction coordinate increases substantially.

In Figure 5, the V_{MEP} is plotted as a function of s, together with the vibrationally adiabatic energy curve, V_a^G [eq 6], which is the MEP incremented by the zero-point energy. Both the QHO and FG ground state are reported here, but they cannot be distinguished on the scale of the figure. The barrier height is found to be 1.2650 eV above the reactants potential energy. As noted above, this is in good agreement with refs 23 and 24. The reaction is found to be slightly exothermic, by about 0.19 eV.

The energy curve, V_a^G, passes through a maximum at the saddle point. It is worthwhile to notice that, while this is true by definition for the MEP, it does not necessarily apply to the curve corrected for the zero-point energy and can be asserted

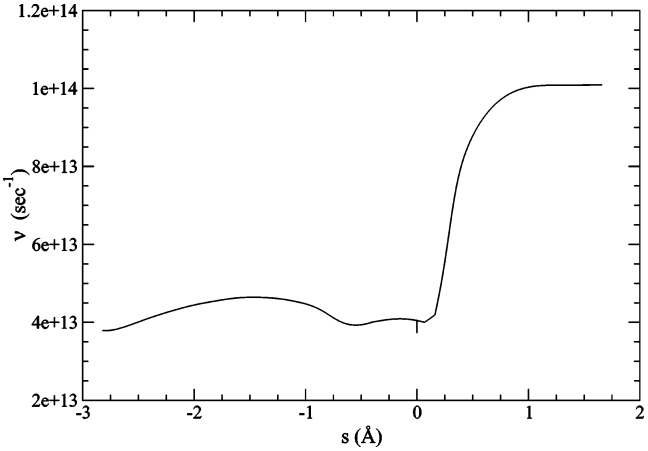

Figure 6. Vibrational frequency of the bound mode orthogonal to the MEP as a function of the reaction coordinate s.

TABLE 1: Rate Constants as a Function of T as Defined in Eq 4 for the Reaction $N_{(ads)} + H_{(ads)} \rightarrow NH_{(ads)}$ on Ru (0001)[a]

T (K)	k^{CHO}	k^{QHO}	k^{FG}	c^{SAG}	c^{SCSAG}	$c^{CVT/QG}$
200	7.71×10^{-19}	1.47×10^{-18}	1.28×10^{-18}	654.38	2848.06	5788.13
250	1.83×10^{-12}	2.75×10^{-12}	2.49×10^{-12}	23.02	39.18	80.47
300	3.26×10^{-8}	4.31×10^{-8}	3.98×10^{-8}	6.63	7.99	17.01
350	3.54×10^{-5}	4.33×10^{-5}	4.06×10^{-5}	3.71	4.02	9.14
400	6.69×10^{-3}	7.80×10^{-3}	7.38×10^{-3}	2.68	2.81	6.72
450	0.39	0.44	0.42	2.19	2.26	5.62
500	1.03×10^{1}	1.13×10^{1}	1.09×10^{1}	1.91	1.95	5.00
550	1.49×10^{2}	1.61×10^{2}	1.55×10^{2}	1.73	1.76	4.61
600	1.37×10^{3}	1.47×10^{3}	1.42×10^{3}	1.61	1.63	4.35
650	9.03×10^{3}	9.53×10^{3}	9.24×10^{3}	1.52	1.53	4.16
700	4.53×10^{4}	4.75×10^{4}	4.61×10^{4}	1.45	1.46	4.01
750	1.83×10^{5}	1.91×10^{5}	1.85×10^{5}	1.39	1.40	3.90
800	6.23×10^{5}	6.46×10^{5}	6.27×10^{5}	1.35	1.36	3.80
850	1.83×10^{6}	1.89×10^{6}	1.84×10^{6}	1.31	1.32	3.72
900	4.79×10^{6}	4.92×10^{6}	4.78×10^{6}	1.28	1.29	3.66
950	1.13×10^{7}	1.16×10^{7}	1.13×10^{7}	1.26	1.26	3.60
1000	2.45×10^{7}	2.50×10^{7}	2.43×10^{7}	1.24	1.24	3.55

[a] All rates are expressed in s^{-1}. Ground-state transmission probabilities calculated by alternative methods are reported in the last three columns.

only as a result of the calculations. We have found that the values of s that minimize the rate constants (eq 4) lie very close to the saddle point in the range of studied temperatures, the maximum distance being approximately 2×10^{-3} Å in the case of the FG method. This indicates that potential energy effects dominate over the zero-point energy effects in determining the location of the generalized TS. This picture could change at higher temperatures.

The vibrational frequency of the normal mode orthogonal to the MEP is plotted in Figure 6 as a function of the reaction coordinate.

Calculated rate constants in the range of temperature from 200 to 1000 K are presented in Tables 1 and 2 for the reaction of H and D, respectively. We find it useful, for purposes of discussion and comparison, to present our results as follows. The first column is the temperature, while second, third, and forth columns are the rate constants calculated according to definition 4. They differ for the expression chosen for the computation of reactants and generalized TS partition functions: CHO stands for classical, QHO for the quantum harmonic approximation, and FG for the full quantum calculation of the vibrational bound states. These rate constants are not corrected for the nonclassical reflection/transmission effects along the reaction coordinate, so they have to be multiplied by the tunneling correction factors shown in the last three columns.

TABLE 2: Rate Constants as a Function of T as Defined in Eq 4 for the Reaction $N_{(ads)} + D_{(ads)} \rightarrow ND_{(ads)}$[a]

T (K)	k^{CHO}	k^{QHO}	k^{FG}	c^{SAG}	c^{SCSAG}	$c^{CVT/QG}$
200	5.45×10^{-19}	7.48×10^{-19}	7.10×10^{-19}	11.72	14.97	30.73
250	1.29×10^{-12}	1.58×10^{-12}	1.52×10^{-12}	3.86	4.08	9.29
300	2.30×10^{-8}	2.64×10^{-8}	2.56×10^{-8}	2.48	2.54	6.16
350	2.50×10^{-5}	2.76×10^{-5}	2.69×10^{-5}	1.96	1.99	5.03
400	4.73×10^{-3}	5.09×10^{-3}	5.00×10^{-3}	1.70	1.72	4.47
450	0.28	0.30	0.29	1.55	1.56	4.12
500	7.29	7.63	7.52	1.44	1.45	3.90
550	1.05×10^{2}	1.09×10^{2}	1.08×10^{2}	1.37	1.38	3.74
600	9.72×10^{2}	1.00×10^{3}	9.91×10^{2}	1.32	1.32	3.62
650	6.39×10^{3}	6.56×10^{3}	6.48×10^{3}	1.28	1.28	3.52
700	3.20×10^{4}	3.28×10^{4}	3.24×10^{4}	1.24	1.25	3.45
750	1.30×10^{5}	1.32×10^{5}	1.31×10^{5}	1.22	1.22	3.39
800	4.41×10^{5}	4.49×10^{5}	4.42×10^{5}	1.19	1.20	3.33
850	1.30×10^{6}	1.32×10^{6}	1.30×10^{6}	1.17	1.18	3.29
900	3.39×10^{6}	3.43×10^{6}	3.38×10^{6}	1.16	1.16	3.25
950	7.99×10^{6}	8.09×10^{6}	7.95×10^{6}	1.15	1.15	3.22
1000	1.73×10^{7}	1.75×10^{7}	1.72×10^{7}	1.13	1.14	3.19

[a] All rates are expressed in s^{-1}. Ground-state transmission probabilities calculated by alternative methods are reported in the last three columns.

The first two are calculated using eq 5 and differ only for the treatment of the reaction path curvature: in the SAG approach, the mass is set to be equal to the H atom mass and curvature is neglected; on the contrary, curvature is included in the SCSAG approach through the use of an effective mass μ_{eff} depending on the reaction coordinate s. Finally, coefficients in the last column include the effect of the quantization of the initial states.

We have also plotted in Figure 7a the transmission probabilities for the title reaction as a function of T, again in the range 200−1000 K. Results yielded by the three employed methods can then be compared. In Figure 7b, we report the ratio of the tunneling coefficients for H and D, again for the three considered methods.

Tables 1 and 2 provide a measure of the importance of treating quantum mechanically the vibrational bound mode orthogonal to the MEP. As expected, effects are more marked for H than for D and become smaller as the temperature increases. For the reaction of H, at 200 K there is a factor of 2 between the classical and the quantum rate, which reduces to a small percent at 1000 K (second and third columns of Table 1). The effect of performing a full quantum calculation is even smaller: the introduction of the anharmonicity causes a change that is never larger than about 10%.

While quantum effects on the bound mode orthogonal to the MEP do not play a significant role, those along the MEP are proved to be much more important. The tunneling factors enhance significantly the rates at low temperatures: at 200 K, for the reaction of H, we find coefficients as large as 654, 2848, and 5788 for the SAG, SCSAG, and CVT/QG methods, respectively. These numbers drastically reduce to 23, 39, and 80 at $T = 250$ K. The SAG and SCSAG approaches show significant differences only for low temperatures: at 350 K, the difference is smaller than 10%.

On the other side, to provide an accurate estimate of the transmission coefficient, it seems to be very important to overcome the continuum approximation in eq 5. The two formulas provide close results if the integrand at the numerator is peaked at energies greater than V_a^{AG}, because in this case the most significant contributions to the coefficient come from the range of energy that is treated in the same way. However, this is not the case for the reaction investigated here: we have verified that the integrand peaks in a range going from ∼1 eV (200 K) to ∼1.35 eV (1000 K). Consequently, quantization of the initial states cannot be safely neglected, as proved by the coefficients reported in the last column of Table 1. At 1000 K, $c^{CVT/QG}$ is three times larger than c^{SCSAG}.

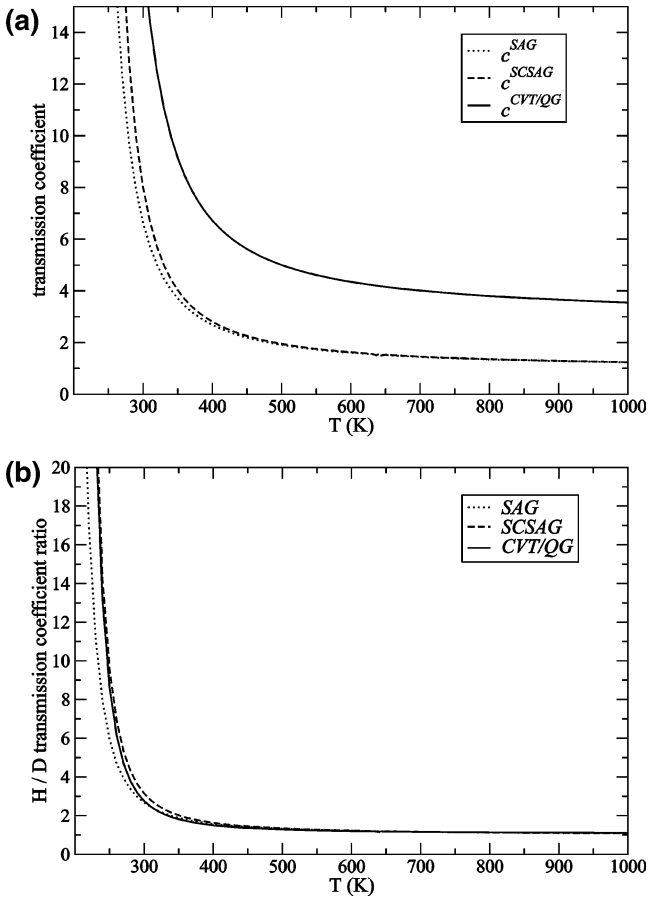

Figure 7. (a) Transmission coefficients for the title reaction calculated with three different levels of theory and reported as a function of the temperature and (b) ratio of the transmission coefficients for the reaction of H and of the isotopic variant D.

Let us now turn the attention on the isotopic variant of the reaction. Table 2 confirms the same trends discussed for H, apart from the obvious generalized reduction of the quantum effects. It is interesting to compare the entirely classical rate constants CHO for the reaction of H and D. Lauderdale and Truhlar, starting from the expression of the partition functions, have derived simple relations to explain the isotopic effect on rate constants (see eqs 43 and 44 of ref 42). In particular, they showed that the ratio of the partition functions for the generalized TS and for the reactants exhibits a dependence on the inverse of the square root of the mass of the moving atom. As a consequence, classical rates are connected by the relation $k_H^{CHO} = (m_D/m_H)^{1/2} k_D^{CHO} = 1.41 k_D^{CHO}$. The same relation holds for quantum rates for high temperatures, while the H/D ratio becomes larger at lower temperatures because, in this case, the ratio of the quantal vibrational partition functions entering eq 3 depend on the isotopic mass via an exponential factor, rather than as $m^{-1/2}$.

These conclusions fully explain our results: the isotopic effect can be quantified as a ratio equal to 1.41 for the entirely classical CHO rate constants, as well as for the quantal ones at high T (compare Tables 1 and 2). Then this ratio progressively increases for quantal rates as the temperature goes down, according to the exponential dependence on the mass for the ratio of the quantal vibrational partition functions.

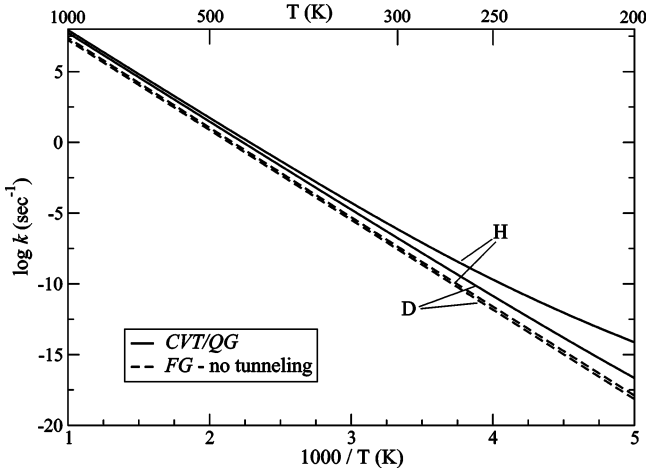

Figure 8. Arrhenius plot for the title reaction and isotopic variant in the range of temperature 200−1000 K. For each reaction, rates not including tunneling effects (FG) are compared with those corrected for quantal effects along the reaction coordinate (CVT/QG).

TABLE 3: Arrhenius Parameters for the Title Reaction and Isotopic Variant with and without Tunneling Corrections Extracted in the Range of Temperature 300−1000 K[a]

	A	E_a
	Hydrogen	
FG	5.13×10^{13}	1.26
CVT/QG	9.85×10^{13}	1.21
	Deuterium	
FG	3.89×10^{13}	1.26
CVT/QG	9.38×10^{13}	1.24

[a] Preexponential factors A in s^{-1}; activation energies E_a in eV.

The isotopic difference between the two reactions is enhanced by the tunnel coefficient: at 200 K, the transmission probability for H is about 190 times bigger. Of course, this effect is quenched as T increases and the tunneling mechanism becomes less important.

Because, as noted above, the system investigated here has a noticeable importance in the industrial production of ammonia, it could be useful to provide the Arrhenius parameters for the rate constants. This would be an easy-to-use tool, for instance, to enter rate constants into kinetic models. To this purpose, we can consider the range of temperature 300−1000 K, which includes the T of 700 K at which usually the ammonia synthesis is performed. In addition, it leaves out the region of T where quantum effects, which cannot be interpreted in the framework of the Arrhenius scheme, are more significant.

In Figure 8, we report the Arrhenius plot for reaction 1 and the isotopic variant. Rate constants refer to the most accurate level of theory provided here, that is, FG for rates with no tunneling corrections and CVT/QG for rates including quantum effects along the MEP. It is evident that plots are four straight lines that can be very nicely fitted by the Arrhenius expression $k = A \exp(-\beta E_a)$, where A is the preexponential factor and E_a is the activation energy. Deviations from linearity are found only for T smaller than 300 and will not be included in the linear regressions. Resulting Arrhenius parameters are given in Table 3. As expected, activation energies are in all cases numerically very close to the actual potential barrier encountered along the MEP of the reaction (1.26 eV).

It is also possible to give an interpretation for the Arrhenius preexponential factor. In the initial state, with H adsorbed in the fcc site, the system can be described in terms of two vibrational normal modes. The mode with lower frequency is mainly along R and is the one that becomes the motion along the MEP, leading to reaction. This vibrational frequency should then provide an estimate of the frequency at which the atom leaves its site to undergo reaction. This is basically the physical interpretation in the present case of the Arrhenius preexponential factor A in Table 3, so it might be possible to establish some kind of connection between A and the vibrational frequency of the normal mode. Indeed, we have calculated this frequency, which turns out to be $\nu = 2.06 \times 10^{13}\ s^{-1}$. This value is close to the value of A calculated in the FG method, $A = 5.13 \times 10^{13}\ s^{-1}$, supporting the idea that the preexponential factor could be reasonably predicted by the frequency of the mode that initiates the reaction.

There is a final issue that needs to be addressed. For the TST scheme of reaction to be valid, the time that the adsorbed atom spends in his site before reacting (τ_{reac}) must be long compared to the time τ_{vib} needed for vibrational relaxation in the site itself. In other words, the scale of time for "vibrational equilibrium" to take place must be much shorter than that for the surface reaction to happen.

The period τ_{reac} can be estimated as the reciprocal of the rate constant. We will then consider the worst possible case corresponding to the highest investigated temperature of 1000 K. This, choosing again the CVT/QG results (last line of Table 1), yields $\tau_{reac} = 1.16 \times 10^{-8}$ s. As for the relaxation, the frequencies above give τ_{vib} on the order of 10^{-14} s for the reactants normal modes, several orders of magnitude smaller than τ_{reac}. The same order of magnitude is found for the TS (see Figure 6, the frequency at the saddle point is numerically close to the ones of the reactants). This ensures us that TST provides a reliable framework for the calculations of rate constants for the present system and in the considered range of temperatures.

5. Conclusions

The TST has provided us with a suitable framework to compute rate constants including quantum transmission effects for a quite complex surface reaction involving 2 coadsorbates and 12 substrate metal atoms. To make a tractable model, we have used a reduced dimensionality approach in which the reaction is essentially described as a migration in a two-dimensional space of the H atom from the initial to the final site. Despite this simplification, we have obtained a barrier height very close to the one estimated by full-dimensional approaches. This ensures us that the chosen coordinates are able to provide a realistic description of the process. Calculated rate constants can be accurately fitted (at least in the range of temperature 300−1000 K) by the Arrhenius expression the parameters of which have been given in Table 3 for different levels of theory and for the two investigated isotopic variants of the reaction.

As a result of our calculations, we notice that quantal effects along the reaction coordinate, especially tunneling through the ground vibrationally adiabatic energy curve, are much more important than those orthogonal to the MEP. It is remarkable that the entirely classical picture provides a reasonably good description of the rate constants: the difference between the CHO and QHO approach is about a factor of 2 at 200 K, which reduces to a very small percent when the temperature is as high as 1000 K. A full quantum treatment including anharmonicity for the bound mode orthogonal to the MEP yields basically results very close to those of the harmonic oscillator approximation in the range of investigated temperatures.

The incidence of tunneling corrections increases dramatically when temperature goes down from 1000 to 200 K: in the case

of SCSAG and CVT/QG the tunneling coefficients gain over 3 orders of magnitude. The effect is less pronounced if the reaction path curvature is neglected. The latter approximation works well at high temperature, when tunneling is not a main mechanism for the reaction but underestimates the transmission effects by a factor of 4 for temperature as low as 200 K. The consideration of the quantization of the initial states plays an important role, basically because of the height of the potential barrier compared to the investigated temperatures. Neglecting this feature causes an underestimate of the tunneling coefficient by a factor equal to 2 or more in the entire range of temperatures.

If it is true that the TST provides a viable way to estimate rate constants, we have also to keep in mind that the theory applied here relies on a series of assumptions and approximations. First of all, we assume a fast equilibration with the products. If this does not occur, the recrossing phenomenon could be important, and the computed rates would be overestimated. This approximation is intrinsic in the TST scheme, and to overcome this picture it would be necessary to perform some kind of molecular dynamics study.

We have also assumed a rigid substrate: the Ru atoms of the metal surface are not allowed to relax in our model. This is of course an approximation: the adsorbed atoms can induce relaxation or deformation on the lattice. In addition, energy exchanges between the adsorbates and the substrate are possible and could be an effective mechanism in enhancing the reaction rates. It might be possible to refine the theory employed here to include some of these effects: for instance, the geometry of the unit cell (at least the first layer) could be optimized, and the kinetic energy of the surface atoms could be included in the reaction path Hamiltonian. These modifications could be performed within the same framework provided by the present approach. The inclusion of phonons would be another possible improvement, but this would require a more general model.

There are also issues that are specific to the synthesis of ammonia. As mentioned in the Introduction, the process is normally carried out at very high pressure, so coverage effects could play some nonnegligible role in the actual synthesis reaction. Also, the presence of steps on the surface of the catalysts could to some extent influence the rates for the process investigated here, even though this is expected to be a much weaker effect than it is for other steps of the synthesis (see section II), such as the dissociative adsorption of the N_2 molecule.

When we look at the number of adopted approximations, it is clear that much needs to be done to achieve the goal of fully explaining the synthetic process of ammonia, and this first step in particular. This is often the case when complex systems involving an high number of atoms are investigated. Nevertheless this work represents a realistic attempt to shed light on the kinetics of one of the key steps of this crucial industrial process. The rate constants provided here in form of Arrhenius law could be easily insert into kinetic models used to achieve a better comprehension of the overall synthetic process.

We can also point to possible future improvements of the work presented here. The first logical step would be to include the second angular variable (accounting for rotation of the H atom parallel to the metal surface) that has been frozen in this work. Reference 23 has identified the existence of alternative reaction paths, indicating a large degree of freedom for H at the transition state. This aspect could be explored in our model by overcoming the two-dimensional approximation and evaluating how the rate constants are affected by the inclusion of this extra coordinate. The only drawback is the amount of computer time for the calculation of the PES, which would become a function of three coordinates. However, the formalism of the variational TST would be unchanged, and the generalization of our code is very straightforward.

It would be also interesting to perform a more detailed dynamical study, possibly by a wave packet calculation. This would be a rigorous treatment of all of the quantum effects of the system and would eliminate the recrossing problem, giving a precise indication on the reliability of the method used here for application to surface reactions.

Acknowledgment. A number of useful discussions with Dr. Massimo Mella are gratefully acknowledged. We thank Dr. Ashildur Logadottir for sending us the preprint of her paper and some unpublished results. Financial support was provided by the European Union Research Training Network, Grant HPRN-CT-2002-00170, "Predicting catalysis: understanding ammonia production from first principles".

References and Notes

(1) Thomas, J. M.; Thomas, W. J. *Principles and Practice of Heterogeneous Catalysis*; VCH: Weinheim, Germany, 1997.
(2) Duley, W. W.; Williams, D. A. *Interstellar Chemistry*; Academic Press: London, U.K., 1984.
(3) Boudart, M. *Handbook of Heterogeneous Catalysis*; Ertl, G., Knözinger, H., Weitkamp, J., Eds.: Wiley-VCH: Weinheim, Germany, 1997: Vol. 1.
(4) Aika, K.; Hori, H.; Ozaki, A. *J. Catal.* **1972**, *27*, 424.
(5) Uchiyama, S.; Hattori, Y.; Ozaki, A.; Aika, K. *Chem. Lett.* **1981**, *10*, 1463.
(6) Shi, H.; Jacobi, K.; Ertl, G. *J. Chem. Phys.* **1993**, *99*, 9248.
(7) Dietrich, H.; Geng, P.; Jacobi, K.; Ertl, G. *J. Chem. Phys.* **1996**, *104*, 375.
(8) Dietrich, H.; Jacobi, K.; Ertl, G. *J. Chem. Phys.* **1996**, *105*, 8944.
(9) Jacobi, K.; Dietrich, H.; Ertl, G. *Appl. Surf. Sci.* **1997**, *121*, 558.
(10) Mortensen, J. J.; Hammer, B.; Nørskov, J. K. *Surf. Sci.* **1998**, *414*, 315.
(11) Mortensen, J. J.; Morikawa, Y.; Hammer, B.; Nørskov, J. K. *J. Catal.* **1997**, *169*, 85.
(12) Hinrichsen, O. *Catal. Today* **1999**, *53*, 177.
(13) Dahl, S.; Sehested, J.; Jacobsen, C. J. H.; Törnqvist, E.; Chorkendorff, I. *J. Catal.* **2000**, *192*, 391.
(14) Romm, L.; Katz, G.; Kosloff, R.; Asscher, M. *J. Phys. Chem. B* **1997**, *101*, 2213.
(15) Diekhöner, L.; Mortensen, H.; Baurichter, A.; Luntz, A. C.; Hammer, B. *Phys. Rev. Lett.* **2000**, *84*, 4906.
(16) Rod, T. H.; Logadottir, A.; Nørskov, J. K. *J. Chem. Phys.* **2000**, *112*, 5343.
(17) Shi, H.; Jacobi, K.; Ertl, G. *J. Chem. Phys.* **1995**, *102*, 1432.
(18) Dahl, S.; Taylor, P. A.; Törnqvist, E.; Chorkendorff, I. *J. Catal.* **1998**, *178*, 679.
(19) Danielson, L. R.; Dresser, M. J.; Donaldson, E. E.; Dickinson, J. T. *Surf. Sci.* **1978**, *71*, 599.
(20) Matsushima, T. *Surf. Sci.* **1988**, *197*, 287.
(21) Dahl, S.; Logadottir, A.; Egeberg, R. C.; Larsen, J. H.; Chorkendorff, I.; Törnqvist, E.; Nørskov, J. K. *Phys. Rev. Lett.* **1999**, *83*, 1814.
(22) Zhang, C.; Liu, Z.-P.; Hu, P. *J. Chem. Phys.* **2001**, *115*, 609.
(23) Zhang, C.; Lynch, M.; Hu, P. *Surf. Sci.* **2002**, *496*, 221.
(24) Logadottir, A.; Nørskov, J. K., submitted for publication, 2003.
(25) Truhlar, D. G.; Garrett, B. C.; Klippenstein, S. J. *J. Phys. Chem.* **1996**, *100*, 12771.
(26) Schwegmann, S.; Seitsonen, A. P.; Dietrich, H.; Bludau, H.; Over, H.; Jacobi, K.; Ertl, G. *Chem. Phys. Lett.* **1997**, *264*, 680.
(27) Jacobi, K. *Phys. Status Solidi A* **2000**, *177*, 37.
(28) Lindroos, M.; Pfnür, H.; Feulner, P.; Menzel, D. *Surf. Sci.* **1987**, *180*, 237.
(29) Ciobîcă, I. M.; Frechard, F.; van Santen, R. A.; Kleyn, A. W.; Hafner, J. *Chem. Phys. Lett.* **1999**, *311*, 185.
(30) Staufer, M.; Neyman, K. M.; Jakob, P.; Nasluzov, V. A.; Menzel, D.; Rösch, N. *Surf. Sci.* **1996**, *369*, 300.
(31) Dietrich, H.; Jacobi, K.; Ertl, G. *Surf. Sci.* **1997**, *377*, 308.
(32) For information and download, see the "Manual for Dacapo" at the website www.fysik.dtu.dk/CAMP/dacapo.html.
(33) Hammer, B.; Hansen, L. B.; Nørskov, J. K. *Phys. Rev. B* **1999**, *59*, 7413.
(34) Vanderbilt, D. *Phys. Rev. B* **1990**, *41*, 7892.
(35) Kresse, G.; Furthmuller, J. *Comput. Mater. Sci.* **1996**, *6*, 15.

(36) Chadi, D. J.; Cohen, M. L. *Phys. Rev. B* **1973**, *8*, 5747.
(37) Skodje, R. T.; Truhlar, D. G.; Garrett, B. C. *J. Phys. Chem.* **1981**, *85*, 3019.
(38) Truhlar, D. G.; Isaacson, A. D.; Skodje, R. T.; Garrett, B. C. *J. Phys. Chem.* **1982**, *86*, 2252.
(39) Truhlar, D. G.; Garrett, B. C. *Annu. Rev. Phys. Chem.* **1984**, *35*, 159.
(40) Truhlar, D. G.; Garrett, B. C. *J. Chim. Phys. Phys.-Chim. Biol.* **1987**, *84*, 365.
(41) Liu, Y.-P.; Lynch, G. C.; Truong, T. N.; Lu, D.-H.; Truhlar, D. G.; Garrett, B. C. *J. Am. Chem. Soc.* **1993**, *115*, 2408.
(42) Lauderdale, J. G.; Truhlar, D. G. *Surf. Sci.* **1985**, *164*, 558.
(43) Truong, T. N.; Truhlar, D. G.; Chelikowsky, J. R.; Chou, M. Y. *J. Phys. Chem.* **1990**, *94*, 1973.
(44) Garrett, B. C.; Truhlar, D. G. *J. Phys. Chem.* **1979**, *83*, 1079.
(45) Pechukas, P. *Annu. Rev. Phys. Chem.* **1981**, *32*, 159.
(46) Colbert, D. T.; Miller, W. H. *J. Chem. Phys.* **1992**, *96*, 1982.
(47) Light, J. C.; Hamilton, I. P.; Lill, J. V. *J. Chem. Phys.* **1985**, *82*, 1400.
(48) Miller, W. H.; Handy, N. C.; Adams, J. E. *J. Chem. Phys.* **1980**, *72*, 99.
(49) Garrett, B. C.; Truhlar, D. G. *J. Chem. Phys.* **1980**, *72*, 3460.
(50) Garrett, B. C.; Truhlar, D. G.; Grev, R. S.; Magnuson, A. W. *J. Phys. Chem.* **1980**, *84*, 1730.
(51) Garrett, B. C.; Truhlar, D. G. *J. Phys. Chem.* **1979**, *83*, 2921.
(52) Skodje, R. T.; Truhlar, D. G.; Garrett, B. C. *J. Chem. Phys.* **1982**, *77*, 5955.